THE ASTROPHYSICAL JOURNAL, 530:L133–L137, 2000 February 20
© 2000. The American Astronomical Society. All rights reserved. Printed in U.S.A.

RINGS IN THE PLANETESIMAL DISK OF β PICTORIS

P. KALAS,[1] J. LARWOOD, [2] B. A. SMITH, [3] AND A. SCHULTZ[1]
Received 1999 September 27; accepted 1999 December 20; published 2000 January 20

ABSTRACT

The nearby main-sequence star β Pictoris is surrounded by an edge-on disk of dust produced by the collisional erosion of larger planetesimals. Here we report the discovery of substructure within the northeast extension of the disk midplane that may represent an asymmetric ring system around β Pic. We present a dynamical model showing that a close stellar flyby with a quiescent disk of planetesimals can create such rings, along with previously unexplained disk asymmetries. Thus we infer that β Pic's planetesimal disk was highly disrupted by a stellar encounter in the last hundred thousand years.

Subject headings: circumstellar matter — planetary systems — stars: individual (β Pictoris)

1. INTRODUCTION

Circumstellar dust disks around nearby stars provide strong indirect evidence for the existence of planetesimals in exosolar systems. Radiation pressure, Poynting-Robertson drag, collisions, and sublimation remove dust orbiting young main-sequence stars on timescales 10^2–10^3 times shorter than the stellar ages (Backman & Paresce 1993). Therefore, we infer that larger parent bodies exist and replenish dust in the same way that comets and asteroids resupply interplanetary grains in the solar system.

We expect that an undisturbed system of many bodies orbiting a star will have an axially symmetric distribution. Over large (10^2 AU) scales, however, the northeast (NE) side of the β Pictoris disk is not a mirror image of the southwest (SW) side (Kalas & Jewitt 1994, 1995). Beginning at ~200 AU (10″) projected radius, the NE disk extension is brighter, longer, and thinner than the SW extension by roughly 20%. Asymmetry is also evident in the disk vertical height; in the SW the disk height is greater north of the midplane than to the south, whereas the opposite is true in the NE extension. The timescale for smoothing such asymmetries is controlled by the orbital period, and it is therefore short relative to the age of the star. Hence the observed asymmetries must be young.

Gravitational perturbation by a brown dwarf companion (Whitmire, Matese, & Tomley 1988) or a close stellar flyby (Kalas & Jewitt 1995) has been suggested as one possible mechanism for generating large-scale disk asymmetry. However, no stellar object physically associated with β Pic has yet been identified. The key problem in identifying a candidate perturber near β Pic is that the star is bright ($V = +3.8$ mag). Even when we artificially eclipse β Pic using a coronagraph, spurious instrumental features that resemble both stars and extended objects dominate optical images. However, data obtained at different telescopes with different instruments have different instrumental noise signatures. We therefore search for the faintest real objects in β Pic's field using optical data from multiple telescopes and instruments.

[1] Space Telescope Science Institute, 3700 San Martin Drive, Baltimore, MD 21218; kalas@stsci.edu.
[2] Astronomy Unit, Queen Mary and Westfield College, London E1 4NS, England, UK.
[3] Institute for Astronomy, University of Hawaii, 2680 Woodlawn Drive, Honolulu, HI 96822.

2. OBSERVATIONS AND RESULTS

Table 1 summarizes the observational data for β Pic. The *Hubble Space Telescope* (*HST*) Archive data consist of WFPC2 CCD images with the β Pic disk oriented along either the Planetary Camera (PC) or the Wide Field Cameras (WFCs). The ground-based observations and data reduction techniques are described in earlier work (Kalas & Jewitt 1995; Smith & Terrile 1984). Here we note that sensitivity to faint objects is hampered by β Pic's bright point-spread function and light from the circumstellar dust disk itself. Both are subtracted using template stars and/or idealized model fits that are detailed in Kalas & Jewitt (1995).

Subtraction of a smooth, symmetric (axially and vertically) model disk reveals a brightness enhancement along the NE extension of the disk midplane 785 AU from the star (feature A; Fig. 1; Table 2). Four field stars common to every data set are utilized for image registration and astrometry, and the feature is confirmed in every data set (except the *HST* PC images, which lack a suitable field of view). We do not detect a similar brightness enhancement anywhere between 25″ and 41″ radius on the SW side of the disk.

The NE disk midplane has several more brightness enhancements between 25″ and 40″ with a degree of positional correlation not present in brightness knots in the field or SW of the star (Fig. 1; Table 2). The centroids of features F and G are spatially correlated to within 0.″5 in the highest resolution images obtained with *HST* and the University of Hawaii 2.2 m telescope. The morphologies and positions of feature centroids vary due to instrumental noise, subpixel registration differences between the observed disk and the idealized model disk, and the number of pixels binned to form a final image. Experiments with the data reduction techniques show that the latter two effects can shift centroids by 1 pixel, which is equivalent to 0.″4–0.″6. These uncertainties are evident even for the highest signal-to-noise detection, feature A (Fig. 1). We identify four more brightness enhancements (B, C, D, and E; Fig. 1) that appear spatially correlated within these uncertainties. We expect that more sensitive, high-resolution observations dedicated to imaging this portion of the disk will help establish the exact number of knots and their positions. Brightness knots near and within the SW disk extension are uncorrelated and can be attributed to noise.

Table 2 gives the measured positions and surface bright-

TABLE 1
OBSERVATIONS

Telescope	Date	Spot Diameter (arcsec)	Pixel Scale (arcsec pixel^{-1})	Central Wavelength (nm)	Integration Time (s)
Las Campanas (2.5 m)	1992 Feb 02	22.5	0.64	647	3900
University of Hawaii (2.2 m)	1993 Oct 12	6.5	0.40	647	655
HST PC (2.4 m)[a]	1995 Dec 12	None	0.05	674	1200
HST WFC (2.4 m)[a]	1995 Oct 15	None	0.10	827	600

[a] *HST* observations do not use a coronagraph. The *HST* PC data have the smallest field of view such that the disk is not detected beyond 32″ radius.

nesses of the seven features. Basic characteristics of the midplane structure are as follows. (1) Feature A at 40.″7 (785 AU) radius is resolved and extended by ~4″ (~80 AU). (2) Feature A shows the greatest enhancement over the mean midplane surface brightness (i.e., displays the greatest contrast). (3) The spacing between features generally increases with increasing radius. (4) The SW disk midplane does not contain comparable features.

We interpret the observed features as dust density enhancements along the projected disk midplane.[4] The density enhancements may represent discrete clouds of dust produced by random planetesimal collisions or a ring system viewed edge-on. We reason that if random planetesimal collisions were important, then we would observe density enhancements on the SW side of the disk also. Because density enhancements are absent in the SW midplane, the random collisions mechanism may be insignificant, although future work should perform quantitative tests.

Here we explore the validity of a ring model to explain the midplane density enhancements. We assume that the multiple features along the NE midplane represent nested eccentric rings viewed close to edge-on. The absence of comparable features to the SW of β Pic means that the rings are not centered on the star. The well-ordered nature of the system of bright features over a radial scale ~300 AU may be indicative of a global restructuring of the planetesimal disk in the recent past. Thus, as a first attempt to explain the origin of such a system, we test how a strong gravitational perturbation, such as from a close stellar flyby, might alter the global morphology of an initially symmetric planetesimal disk. In addition, we require that the resulting disk morphology qualitatively fit the radial and vertical disk asymmetries known to exist along the same region of the disk as the proposed ring system.

3. DYNAMICAL SIMULATIONS

We utilize a standard numerical code[5] (Mouillet et al. 1997) to follow ~10^6 collisionless test particles that are initialized in circular orbits about a point-mass potential; this system experiences an encounter with a secondary point mass that follows a prescribed parabolic trajectory. The key parameters governing the disk response are the mass ratio, the pericenter distance q, and the inclination of pericenter to the initial midplane of the disk i. The test particles are taken to represent the underlying parent bodies that replenish the dust through infrequent collisional disruption. We assume that the distribution of simulated particles traces the distribution of dust grains that

[4] Given the number of faint (23 mag $< m_R <$ 24 mag) objects detected in the entire unobstructed field of view, there is a ~3% chance that one of the disk features is due to a background galaxy.

[5] We assume an initial $r^{-3/2}$ radial dependence of surface number density and a vertically exponential density profile with the disk flared such that the scale height is proportional to $r^{3/2}$.

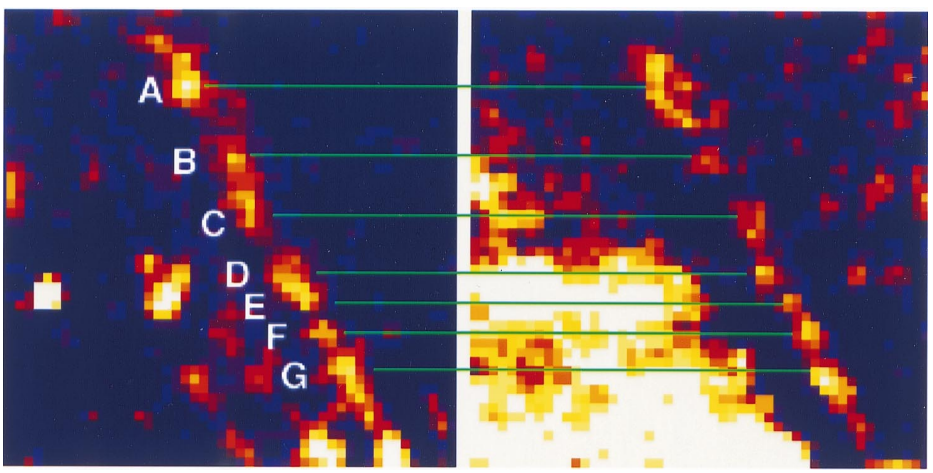

FIG. 1.—Two of the four data sets used to identify real substructure along the NE extension of β Pic. North is up, east is left, and the field of view for each image is 20″ × 20″. The left panel shows the WFC2 data, and the right panel shows the University of Hawaii data (Table 1). Images are registered using field stars located throughout the entire fields of view (roughly 200″ × 200″). The WFC2 data are binned to 0.″4 pixel^{-1} and smoothed with a Gaussian profile having $\sigma = 0.7$ pixel, in order to both match the pixel scale of the University of Hawaii data and increase sensitivity to nebulosity. Originally the images contained the NE extension of β Pic's circumstellar disk. The disk was subtracted using a model of scattered light from a dusty circumstellar disk fit to the global morphology of each disk extension. After subtraction, most of the disk disappears except for radial substructure that is not locally fit by the idealized, smooth model disk. We draw horizontal lines indicating midplane features that appear spatially correlated to within 2 pixels in all the data listed in Table 1. The effects of noise in modulating the position and morphology of features is evident even for the most robust detection, feature A. Features F and G also display 1–2 pixel spatial correlation, but validating the existence and spacing of features B, C, D, and E requires observations with better sensitivity and resolution.

TABLE 2
NORTHEAST DISK MIDPLANE STRUCTURE

Feature	Radius[a] (AU)	Surface Brightness[b] (mag arcsec^{-2})	Enhancement[c] (%)
A	785	23.5	>20
B	710	23.7	10
C	647	24.1	5
D	608	24.0	5
E	575	24.0	5
F	543	24.0	5
G	506	24.0	5

[a] Conversion of radius in arcsec to AU assumes β Pic is 19.3 pc from the Sun. The position of feature A is the measurement of its centroid in unbinned *HST* WFC data (Table 1), with an uncertainty of 5 AU. The positions of features B–G are the averages of measurements made in all the data listed in Table 1, with uncertainties of ~10 AU.

[b] Absolute and relative surface brightnesses are sensitive to small changes in the position and scaling of the axisymmetric model disk used for subtraction. The estimated uncertainties in the surface brightness measurements are $\sigma \sim 0.3$ mag arcsec^{-2} for feature A and $\sigma \sim 0.5$ mag arcsec^{-2} for the other features.

[c] Enhancement is the local contrast between a feature and a least-squares, power-law fit to a 20″ segment of the disk midplane.

would result from collisions in the real system (Mouillet et al. 1997).

We find that coplanar encounters distort disk structure near periastron, leading to the development of transient kinematic spiral features. These are regions of eccentricity growth. Within a few disk orbital periods of periastron passage, the spiral patterns collapse into generally eccentric nested rings. If the encounter timescale is sufficiently short, as in relatively close encounters, then one spiral arm dominates the response. Correspondingly, the disk takes on a lopsided appearance (Larwood 1997). After many orbital periods, the ring patterns become incoherent through orbital phase mixing. Inside a radius ~q/4, the tidal influence of the perturber is slight; outside a radius ~q/3, the interaction rapidly increases in strength (Hall, Clarke, & Pringle 1996). Similarly, non-coplanar flyby encounters excite inclination changes in the orbits of disk particles (Clarke & Pringle 1993), generating asymmetry about the midplane (Ostriker 1994).

The stellar mass ratio is taken to be 0.3 throughout the models presented here. The perturber therefore has the mass of an M star relative to β Pic. However, varying the mass ratio was not found to affect the qualitative outcome significantly compared with varying q. We investigated the induced length asymmetry in the disk as a function of q for coplanar encounters. For a broad range of viewing angles, the required length asymmetry (~20%) is produced at a radius corresponding to the initial size of the disk when q is 1.3 times larger than that value. We then considered various inclinations i for the encounter and compared the resulting isophotal contours with those from observations for various viewing angles.

Figures 2, 3, and 4 present the simulation that best reproduces the observational data. The model disk is seen nine orbital periods (at the initial outer radius) after periastron. Planetesimals have scattered outward to several times the initial disk radius and show well-defined ringed structure on one side of the disrupted disk, but not the other—in agreement with the observations (Fig. 1). In the edge-on view, model disk isophotes qualitatively match the observed asymmetries in length, width, and height above and below the midplane (Fig. 3). The rings appear as bumps along the disk midplane in the edge-on view, with spacing increasing with radius (Fig. 4).

Ring structure inside computational radius 2 has been eliminated by orbital phase mixing, which in the observational data

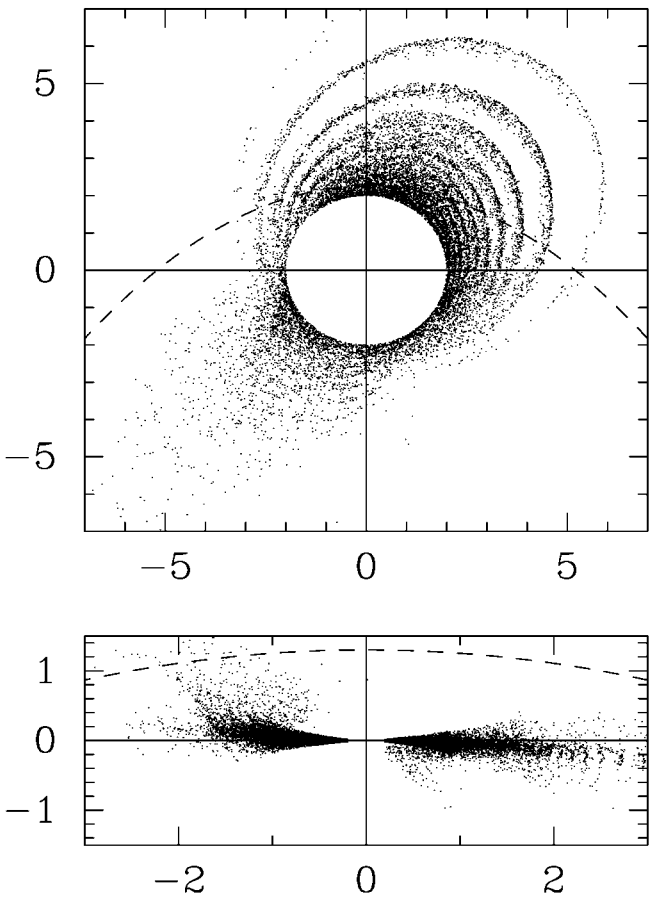

FIG. 2.—Face-on and edge-on views of the simulation particles in the computational frame centered on the β Pic mass. The horizontal axes correspond to the line of nodes of the perturber orbit. Parameters are $q = 2.6$ and $i = 30°$. The disk is initially distributed between 0.2 and 2 radius units. The path of the perturber is indicated with a dashed line and enters the field from the right-hand side. *Top:* The face-on view showing the large-scale structure of the perturbed disk. We plot a random sample of a quarter of the particles outside a radius corresponding to the initial disk extent. The sense of rotation is counterclockwise, the perturber reaching closest approach on the vertical axis. *Bottom:* The edge-on view produced by rotating the top panel 90° about the horizontal axis. One side of the disk is vertically distended and strongly truncated, whereas the opposite side is radially distended with rings. Also, the disk is slightly tilted with respect to its initial configuration (i.e., midplane along the horizontal axis). Viewed with the appropriate orientation, we identify the short and long sides of the disk with β Pic's SW and NE extensions, respectively.

corresponds to radius ~26″ (500 AU). The region of relatively unperturbed particles, q/4, now scales to ~9″, which is consistent with the projected radius at which disk asymmetries are observed to begin (Kalas & Jewitt 1995). Having determined the length unit, we deduce that this model is at a state ~90,000 yr after periastron. Since the removal timescale of dust due to Poynting-Robertson drag is significantly longer than 10^5 yr (Backman & Paresce 1993), the distribution of parent bodies will trace the reflecting dust particles, as we initially assumed.

4. DISCUSSION

The stellar flyby hypothesis provides a simple explanation for the existence, spacing, and morphology of the brightness maxima along β Pic's midplane, as well as the large-scale disk asymmetries. The pumped up velocity dispersion of planetesimals may also lead to increased dust replenishment rates, owing to more frequent and destructive collisions (Stern & Colwell

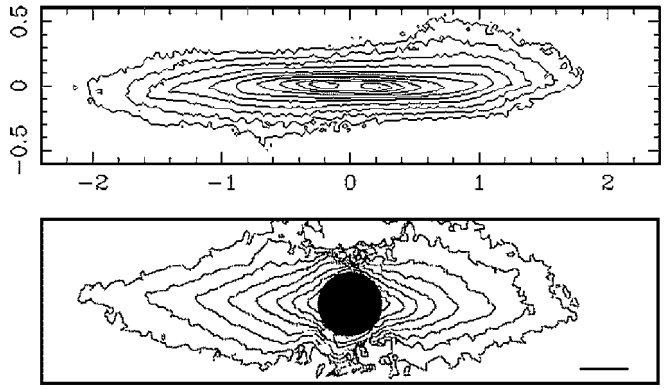

FIG. 3.—*Top*: Isophotal contours for the simulated disk. The contours are created by projecting the particle positions onto a plane perpendicular to the simulated line of sight and binning particles. The brightness for each bin is the sum of contributions from each particle in the bin, assuming isotropically scattered stellar light without extinction. This procedure is used only as a rough guide to the morphology that would be seen in a real system in which the scattering surface is provided by dust supplied from planetesimal collisions. The appearance of these contours was investigated for various viewing angles, and we considered an azimuthal displacement of 165° and inclination to line of sight of 4° to yield the most satisfactory result. We note that the best viewing angles will depend on the details of the scattering phase function, the initial disk model, and the dust evolution model. *Bottom:* The observed surface brightness isophotes of the β Pic disk for the 1993 October 12 coronagraphic data. Isophote spacing is 1 mag arcsec^{-2}, and the outer contour gives 22 mag arcsec^{-2}. The NE extension is oriented to the left-hand side of the occulted star, and the north side of the disk midplane is upwards on the page. The bar represents 5″ (~100 AU). The SW side of the disk is shorter and wider than the NE side, and isophotes extend higher north of the midplane compared to the south.

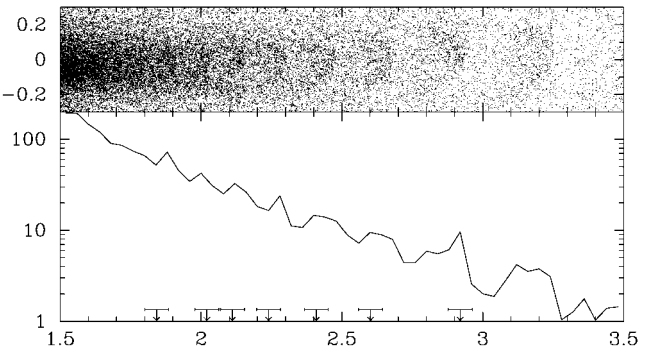

FIG. 4.—*Top:* Close-up view of particles in the simulated NE extension. *Bottom:* Binned brightness profile along the simulated NE extension in the top panel. The brightness for each bin (0.04 × 0.08) was defined by summing $1/r^2$ for each particle in the bin, where r is the correct three-dimensional radius. The brightness unit is computational: brightness from one particle at unit distance = 1. If we associate feature A found in the β Pic disk with the density enhancement at 2.92 in the simulation, then we can explain the radial distribution of all bright features, within observational uncertainty. Arrows indicate real data, appropriately scaled. Error bars give the 0.″6 uncertainty in the radial position measurements as discussed in the text. The density enhancement at radius 3.15 (*bottom*) is not detected in our data. It contains roughly half the particles of feature A, and more sensitive observations are required to test for its presence.

1997; Kenyon & Luu 1999). Therefore, the large total dust mass around β Pic compared to that of other main-sequence stars probably results from both its youth (Barrado y Navascues et al. 1999) and the dynamical state of the system. Our model for β Pic's recent dynamical history implies that the top panel of Figure 2 approximates the face-on view of the planetesimal disk.

The encounter distance assumed in the simulation scales to ~700 AU, implying a statistically unlikely event (0.01% chance in 10^6 yr, assuming empirical parameters for the solar neighborhood; Garcia-Sanchez et al. 1999). However, if β Pic formed with a bound stellar companion on a $\gg$1000 AU radius orbit and it was the companion that was perturbed by a stellar flyby into a new orbit that disrupted the planetesimal disk, then the flyby probability increases by an order of magnitude or more. This scenario is also consistent with the prograde and relatively small angle trajectory of the perturber relative to the disk midplane in our simulation. Ultimately, identification of the perturber is necessary to validate the stellar flyby hypothesis. Future work will present a comprehensive, statistical analysis of the relative space motions and uncertainties for candidate perturbers using *Hipparcos* data (P. Kalas, J.-M. Deltorn, & J. D. Larwood 2000, in preparation).

We note that the orientation of the outer disk height asymmetry is in the same direction relative to the midplane as the proposed midplane warp imaged ~50 AU from the star (Burrows, Krist, & Stapelfeldt 1995). This inner warp could be due to a planet that is inclined relative to the disk midplane (Mouillet et al. 1997). The stellar flyby hypothesis offers an alternate explanation for the warp. The non-coplanar flyby generates planetesimal orbits with increased eccentricity and inclination, which at apastron manifest as the flared disk in the SW extension. However, as seen in the edge-on projection, this family of vertically scattered planetesimals crosses the main disk on its way to periastron at ~50 AU to the NE of β Pic (Fig. 2). This intersecting "second plane" might contaminate isophotes from the quiescent inner disk, giving the appearance of a warped midplane. Hypothetical planets near 50 AU radius may also encounter the second-plane planetesimals and deliver them to the innermost parts of the system, leading to an enhancement of cometary activity (Knacke et al. 1993; Beust et al. 1996).

The main effect of the external perturber is to scatter planetesimals from their formation sites outward to greater radii and vertically away from the midplane. Roughly 10% of the disk mass is actually lost to interstellar space in the simulation presented here.[6] This rearrangement of the planetesimal disk was achieved primarily by the gas giant planets during the evolution of the solar system. However, recent theoretical work links the high eccentricities and inclinations of Kuiper Belt objects to close stellar flybys with the young Sun (Ida, Larwood, & Burkert 2000). The current state of the β Pic system may therefore accurately represent an early evolutionary phase of our solar system.

P. K. and J. L. acknowledge support from both STScI and MPIA-Heidelberg. We thank A. Evans, F. Bruhweiler, C. Burrows, S. Ida, J. Surace, and R. Terrile for contributing to this research. We are grateful to D. Jewitt, D. Backman, S. Beckwith, M. Clampin, and J. Papaloizou for commenting on drafts of the manuscript.

[6] Escaping particles have velocities ~5 km s^{-1}, in which case they could cover the distance between β Pic and the Sun in ~4 Myr.

REFERENCES

Backman, D. E., & Paresce, F. 1993, in Protostars and Planets III, ed. E. H. Levy & J. I. Lunine (Tucson: Univ. Arizona Press), 1253
Barrado y Navascues, D., Stauffer, J. R., Song, I., & Caillault, J.-P. 1999, ApJ, 520, L123
Beust, H., Lagrange, A.-M., Plazy, F., & Mouillet, D. 1996, A&A, 310, 181
Burrows, C. J., Krist, J. E., & Stapelfeldt, K. R. 1995, BAAS, 187, 32.05
Clarke, C. J., & Pringle, J. E. 1993, MNRAS, 261, 190
Garcia-Sanchez, J., Preston, R. A., Jones, D. A., Weissman, P. R., Lestrade, J.-F., Latham, D. W., & Stefanik, R. P. 1999, AJ, 117, 1042
Hall, S. M., Clarke, C. J., & Pringle, J. E. 1996, MNRAS, 278, 303
Ida, S., Larwood, J., & Burkert, A. 2000, ApJ, 528, 351
Kalas, P., & Jewitt, D. 1994, in Circumstellar Dust Disks and Planet Formation, ed. R. Ferlet & A. Vidal-Madjar, (Gif sur Yvette: Editions Frontières), 371
Kalas, P., & Jewitt, D. 1995, AJ, 110, 794
Kenyon, S. J., & Luu, J. X. 1999, AJ, 118, 1101
Knacke, R. F., Fajardo-Acosta, S. B., Telesco, C. M., Hackewell, J. A., Lynch, D. K., & Russel, R. W. 1993, ApJ, 418, 440
Larwood, J. D. 1997, MNRAS, 290, 490
Mouillet, D., Larwood, J. D., Papaloizou, J. C. B., & Lagrange, A.-M. 1997, MNRAS, 292, 896
Ostriker, E. C. 1994, ApJ, 424, 292
Smith, B., & Terrile, B. 1984, Science, 226, 1421
Stern, S. A., & Colwell, J. E. 1997, ApJ, 490, 879
Whitmire, D. P., Matese, L. J., & Tomley, L. J. 1988, A&A, 203, L13